

1 **Freshwater discharge controlled deposition of**
2 **Cenomanian-Turonian black shales on the NW European**
3 **epicontinental shelf (Wunstorf, North Germany)**

4
5 **N.A.G.M. van Helmond¹, A. Sluijs¹, J.S. Sinninghe Damsté^{2,3}, G.-J. Reichart^{2,3}, S.**
6 **Voigt⁴, J. Erbacher⁵, J. Pross⁶, H. Brinkhuis^{1,3}**

7
8 [1]{Marine Palynology and Paleoceanography, Laboratory of Palaeobotany and Palynology,
9 Department of Earth Sciences, Faculty of Geosciences, Utrecht University, Budapestlaan 4,
10 3584 CD Utrecht, Netherlands }

11 [2]{Department of Earth Sciences, Faculty of Geosciences, Utrecht University, Budapestlaan
12 4, 3584 CD Utrecht, Netherlands }

13 [3]{NIOZ, Royal Netherlands Institute for Sea Research, P.O. Box 59, 1790 AB Den Burg,
14 Texel, Netherlands }

15 [4]{Institute of Geosciences, Goethe-University Frankfurt, Altenhöferallee 1, 60438
16 Frankfurt, Germany }

17 [5]{Bundesanstalt für Geowissenschaften und Rohstoffe, P.O. Box 51 01 53, Alfred-Benz-
18 Haus, Stilleweg 2, 30641 Hanover, Germany }

19 [6]{Paleoenvironmental Dynamics Group, Institute of Earth Sciences, University of
20 Heidelberg, Im Neuenheimer Feld 234, 69120 Heidelberg, Germany }

21 Correspondence to: N.A.G.M. van Helmond (n.vanhelmond@uu.nl)

22
23 **Abstract**

24 Global warming, changes in the hydrological cycle and enhanced marine primary productivity
25 all have been invoked to have contributed to the occurrence of widespread ocean anoxia
26 during the Cenomanian-Turonian Oceanic Anoxic Event (OAE2; ~94 Ma), but disentangling
27 these factors on a regional scale has remained problematic. In an attempt to separate these
28 forcing factors, we generated palynological and organic geochemical records using a core
29 spanning the OAE2 from Wunstorf, Lower Saxony Basin (LSB; North Germany), which
30 exhibits cyclic black shale – marl alternations related to the orbital precession cycle.

31 Despite the widely varying depositional conditions complicating the interpretation of the
32 obtained records, TEX₈₆^H indicates that sea-surface temperature (SST) evolution in the LSB
33 during OAE2 resembles that of previously studied sites throughout the proto-North Atlantic.

1 Cooling during the so-called Plenus Cold Event interrupted black shale deposition during the
2 early stages of OAE2. However, TEX_{86} does not vary significantly across marl-black shale
3 alternations, suggesting that temperature variations did not force the formation of the cyclic
4 black shale horizons. Relative (i.e., with respect to marine palynomorphs) and absolute
5 abundances of pollen and spores are elevated during phases of black shale deposition,
6 indicative of enhanced precipitation and run-off. High abundances of cysts from inferred
7 heterotrophic and euryhaline dinoflagellates supports high run-off, which likely introduced
8 additional nutrients to the epicontinental shelf resulting in elevated marine primary
9 productivity.

10 We conclude that orbitally-forced enhanced precipitation and run-off, in tandem with elevated
11 marine primary productivity, were critical in cyclic black shale formation on the northwest
12 European epicontinental shelf and potentially for other OAE2 sections in the proto-Atlantic
13 and Western Interior Seaway at similar latitudes as well.

14

15 **1 Introduction**

16 Dark, often laminated marine sediments that are usually devoid of fossil traces of benthic life
17 and exhibit a total organic carbon (TOC) content of $>1\%$ (Creaney and Passey, 1993), were
18 episodically deposited during Jurassic and Cretaceous times. The deposition of these
19 sediments, generally referred to as black shales, has typically been taken to indicate ancient
20 episodes of dys- or anoxic bottom water conditions (Schlanger and Jenkyns, 1976). During
21 some of these episodes, anoxia developed widespread in one or more ocean basins; such
22 episodes were termed Oceanic Anoxic Events (OAEs; Schlanger and Jenkyns, 1976). One of
23 the most prominent, best-constrained and best-studied of these OAEs formed across the
24 Cenomanian-Turonian boundary (CTB; ~ 94 Ma) and became known as OAE2 (e.g., Jenkyns,
25 2010). The widespread enhanced organic carbon burial in marine sediments during OAE2 is
26 expressed by a worldwide documented $>2\text{‰}$ positive carbon isotopic excursion (CIE) of
27 carbonate ($\delta^{13}\text{C}_{\text{carb}}$) and organic matter ($\delta^{13}\text{C}_{\text{org}}$), with an estimated duration of 450-600 kyr
28 (e.g., Voigt et al., 2008; Meyers et al., 2012). This CIE likely resulted from enhanced burial of
29 $\delta^{13}\text{C}$ -depleted organic matter (Arthur et al., 1988; Tsikos et al., 2004) and therefore provides a
30 C-isotopic signature of the global exogenic carbon pool, making it a proper tool to confidently
31 correlate OAE2 sections.

32 Over the past decades, many studies have been conducted to unravel the processes responsible
33 for this massive burial of organic carbon during OAEs, and OAE2 in particular. Extensive
34 volcanism close to the CTB (e.g. Snow et al., 2005; Kuroda et al., 2007; Turgeon and Creaser,

1 2008) has been linked to high levels of atmospheric CO₂ (e.g., Schouten et al., 2003;
2 Sinninghe Damsté et al., 2008; Barclay et al., 2010), raising the temperatures of already warm
3 oceans towards a maximum at the onset of OAE2 (e.g., Bice et al., 2006; Forster et al., 2007),
4 which reduced the solubility of oxygen in surface waters. This warming caused an enhanced
5 hydrological cycle (van Helmond et al., 2014), which would likely have contributed to
6 increased rates of continental weathering and runoff (Blätter et al., 2011; Pogge von
7 Strandmann et al., 2013). This, in turn would have led to at least seasonal stratification and
8 enhanced nutrient supply to continental margins and epicontinental seas. Extensive volcanism
9 may also have directly contributed to ocean fertilization (Kerr et al., 1998; Snow et al., 2005),
10 while changes in proto-Atlantic circulation may have increased the strength of upwelling
11 (e.g., Poulsen et al., 2001; Junium and Arthur, 2007). Enhanced regeneration of sedimentary
12 phosphorus from dysoxic and anoxic sediments (e.g., Kuypers et al., 2004b; Mort et al., 2007)
13 combined with abundant nitrogen-fixing cyanobacteria (Kuypers et al., 2004b) may have
14 sustained high levels of primary productivity. All of the above factors would conspire to
15 expansion of oxygen minimum zones and oxygen depletion of bottom waters, leading to
16 enhanced organic carbon burial.

17 As a result of late Cenomanian sea level rise (e.g., Erbacher et al., 1996; Voigt et al., 2006),
18 large parts of continents became flooded, greatly expanding the extent of epicontinental shelf
19 seas where sediments recording the OAE2 were deposited. Particularly the Lower Saxony
20 Basin (LSB; northwest Germany) exhibits expanded and complete OAE2-succesions
21 (Wilmsen, 2003) containing several cyclic alternations of organic-poor marls, limestones and
22 organic-rich black shales (Voigt et al., 2008). Organic matter accumulation on the European
23 shelf was relatively modest, however, compared with other cyclic OAE2-sections in the
24 proto-Atlantic (Kuypers et al., 2004a; Forster et al., 2008).

25 The complete OAE2-interval has been recovered from the LSB through coring at Wunstorf
26 (Erbacher et al., 2007; North Germany; Fig. 1). Application of an orbital cycle-based age
27 model has shown that black shale deposition in the Wunstorf core sediments is consistent with
28 precession forcing (Voigt et al., 2008). This implies that climate change resulting from orbital
29 fluctuations was directly related to phases of black shale deposition. The robust
30 cyclostratigraphy and biostratigraphic zonation of the Wunstorf core allows for a high-
31 resolution study of astronomically-induced climate change. Here we aim to reconstruct mean
32 annual sea surface temperature (SST), hydrological changes and marine primary productivity,
33 to determine the dominant control on decreasing oxygen concentrations during OAE2 on the
34 European shelf. To this end, we combined organic geochemical (TEX₈₆; BIT index) and

1 palynological proxies, notably organic-walled dinoflagellate cysts (dinocysts) and pollen and
2 spore abundances, across the CTB for the Wunstorf core.

3 4 **2 Material and methods**

5 **2.1 Site description, depositional setting and age model**

6 The Wunstorf core was drilled in 2006 ~25 km west of Hannover, Germany (52°24.187'N,
7 9°29.398'E, Voigt et al., 2008; Fig.1). Approximately 76 m of middle Cenomanian to middle
8 Turonian sediments, comprising a ~13.5 m thick CTB succession, were retrieved. During the
9 Late Cretaceous, the drill site was located in the LSB, which was part of the expanded
10 epicontinental shelf sea that covered most of Eurasia after the Cenomanian transgression
11 (Hancock and Kauffman, 1979). The sediments at Wunstorf were deposited at an estimated
12 water depth of 100-150 m based on sequence stratigraphy, sedimentological analysis and
13 (micro)fossil content (Wilmsen, 2003). The most proximal exposed land, the Rheno-Bohemian
14 Massif, was located ~150 km to the south and formed a barrier towards the Western Tethys.
15 The Armorican and British massifs formed a barrier towards the Atlantic, while the
16 Fennoscandian Shield formed a barrier to the open ocean in the north (Fig.1; Wilmsen, 2003).
17 The OAE2-interval at Wunstorf is part of the Hesseltal Formation and occurs between 49.6
18 and 23.1 meters below surface (mbs). The Hesseltal Formation consists of rhythmically
19 alternating couplets of finely laminated black shales with elevated levels of total organic
20 carbon (TOC; max. 2.8%; Hetzel et al., 2011; Fig. 2b), grey to green marls, and light-grey
21 (marly) limestones (Fig. 2; Erbacher et al., 2007; Voigt et al., 2008). The cyclic lithology
22 results from a depositional system greatly influenced by precession (Voigt et al., 2008).
23 Biostratigraphic zonation for the Hesseltal Formation relies on inoceramids, ammonites, acme
24 occurrences of macrofossils and planktonic foraminifera that can be reliably correlated
25 regionally and globally (Ernst et al., 1984; Voigt et al., 2008, and references therein).
26 The onset of the OAE2-interval is primarily based on the first occurrence (FO) of the
27 ammonite *Metoicoceras geslinianum* at 49.6 mbs, consistent with the English Chalk (Voigt et
28 al., 2008). At 47.8 mbs, the onset of the characteristic positive shift in $\delta^{13}\text{C}_{\text{carb}}$ (~2‰) and
29 $\delta^{13}\text{C}_{\text{org}}$ (~2.5‰) was recognized (Voigt et al., 2008; Du Vivier et al., 2014; Fig. 2a). The
30 termination of the OAE2 interval at Wunstorf was placed at 36 mbs (Voigt et al., 2008). The
31 duration of the OAE2 for the Wunstorf core was estimated at ~435 kyr or ~500 kyr based on
32 spectral analyses of the lithological cyclicity and $\delta^{13}\text{C}_{\text{org}}$, respectively (Voigt et al., 2008; Du
33 Vivier et al., 2014).

2.2 Total organic carbon analysis

About 0.3 g of freeze-dried and powdered sediment sample was decalcified using 1M HCl, followed by rinsing with demineralized water and drying again. Total Organic Carbon (TOC) concentrations were measured using a Fisons Instruments CNS NA 1500 analyzer and corrected for weight loss during decalcification. Results were normalized to in-house standards, acetanilide, atropine and nicotinamide. The average analytical uncertainty based on duplicate analyses of sediment samples was 0.04 weight percent (wt.%).

2.3 Organic geochemistry

For 48 samples, biomarkers were extracted from 10-15 g of powdered and freeze-dried sediments with a Dionex accelerated solvent extractor (ASE) using dichloromethane (DCM)/methanol mixture (9:1, v/v). Total lipid extracts (TLEs) were evaporated to near dryness using rotary evaporation. Subsequently, remaining solvents were removed under a nitrogen flow. The TLEs were separated by Al₂O₃ column chromatography, into apolar, ketone, glycerol dialkyl glycerol tetraether (GDGT) and polar fractions using three column volumes of the eluents hexane/DCM (9:1, v/v), ethyl acetate (v), DCM/methanol (95:5, v/v) and DCM/methanol(1:1, v/v), respectively. The apolar and GDGT fractions were dried under a nitrogen flow and weighed. The apolar fractions of two samples (41.14 mbs and 42.81mbs), selected based on their high yield, were measured using gas chromatography-mass spectrometry (GC-MS), to determine the thermal maturity of the sediments based on the degree of isomerisation of hopanes. Only two samples were analyzed because it is very unlikely that the degree of thermal maturity will change over a distance of 25 m (difference in depth of the studied section). This relates to the relatively modest geothermal gradient of 2.5°C per 100 m. Analyses were performed on a Thermo Finnigan Trace Gas Chromatograph (GC) Ultra connected to a Thermofinnigan DSQ mass spectrometer operated at 70 eV, with a range of m/z 50–800 and a cycle time of 3 scans s⁻¹. The temperature program and column conditions resemble that of Sinninghe Damsté et al. (2008). To quantify the GDGT abundances a known amount of C₄₆ GDGT-standard was added (Huguet et al., 2006), after which the GDGT-fractions were re-dissolved in hexane/propanol (99:1, v/v) and filtered over a 0.45 µm mesh PTFE filter. The filtered GDGT fractions were analysed using high performance liquid chromatography - atmospheric pressure chemical ionization/ mass spectrometry (HPLC-APCI/MS) according to the method described in Schouten et al. (2007a). Analysis were performed on an Agilent 1290 infinity series coupled to a 6130 single quadrupole MSD, equipped with auto-injection system and HP-Chemstation software.

1 Separation was achieved on a Prevail Cyano column (150 mm x 2.1 mm, 3 μm ; Alltech).
2 GDGTs (m/z 1018-1302) were detected using selective ion monitoring. For this method it was
3 exhibited that for samples with a high TEX_{86} value, a concentration of 0.1 ng of injected
4 GDGTs on the LC column was still sufficient to yield trustworthy TEX_{86} values (Schouten et
5 al., 2007a). The minimum GDGT concentration injected on the LC column per measurement
6 in this study was ~ 0.3 ng. TEX_{86} -index values were calculated after Schouten et al. (2002),
7 and converted to absolute annual average sea surface temperatures (SSTs) using the $\text{TEX}_{86}^{\text{H}}$
8 Kim et al. (2010) modern core top calibration, which has a calibration error of 2.5°C .
9 Analytical reproducibility was generally better than 0.3°C .
10 The Branched and Isoprenoid Tetraether (BIT) index was used to estimate the relative
11 abundance of soil organic matter in marine sediments (Hopmans et al., 2004). The BIT index
12 is based on the amount of predominantly soil-derived branched GDGTs (brGDGTs) relative
13 to the isoprenoid GDGT (iGDGT) crenarchaeol, which is chiefly derived from marine
14 Thaumarchaeota. Application of the BIT index may be complicated by in situ production of
15 brGDGTs in the marine water column and in marine sediments and the ubiquitous presence of
16 crenarchaeol in soils. Nonetheless many studies have shown that the BIT index is still a useful
17 tracer for continental organic matter in marine environments (Schouten et al., 2013).

18

19 **2.4 Palynology**

20 In total 51 samples were prepared for quantitative palynological analysis. In general between
21 5 and 10 g, and for samples low in organic carbon up to ~ 20 g, of freeze-dried sediment
22 sample were crushed to pieces smaller than 5 mm. Subsequently a known amount of
23 *Lycopodium* marker spores was added to allow for quantitative analysis. After reaction with
24 $\sim 30\%$ HCl and twice with $\sim 38\%$ HF, to dissolve carbonates and silicates respectively,
25 ultrasonic separation was employed. Finally, samples were sieved over a $15 \mu\text{m}$ nylon mesh.
26 Residuals were mounted on slides for microscopic analysis. Approximately 250 dinocysts per
27 sample were counted using a light microscope at 500x magnification. Taxonomy follows that
28 of Fensome and Williams (2004). Pollen and spores were counted as one group, except for
29 saccate gymnosperm pollen. All samples and slides are stored in the collection of the
30 Laboratory of Palaeobotany and Palynology, Utrecht University, the Netherlands.

31

32 **3 Results**

33 **3.1 Total organic carbon**

1 Trends in, and absolute values of TOC (Fig. 2) are generally in agreement with results
2 reported by Hetzel et al. (2011), i.e., relatively high for black shales and low for marls and
3 limestones. The background TOC content is <0.3%, somewhat higher than reported by Hetzel
4 et al. (2011). Within the OAE2, four intervals with elevated TOC content are identified. The
5 first interval is between 49 and 47.5 m and contains the first black shale, at the onset of the
6 CIE. A second organic-rich cluster is recognized between ~44 and 42 mbs, with the maximum
7 TOC content approaching 2%. The third organic-rich interval is from 41 to 39.5 mbs, with a
8 maximum TOC content just over 2.5%. The last organic-rich cluster ranges from 37.5 to 35.5
9 mbs, with a maximum TOC content just above 2%. For the remainder of the record, only the
10 youngest sample (26.51 mbs) has an elevated TOC content (close to 1.5%).

11

12 **3.2 Thermal maturity**

13 For two selected samples the hopane distribution was determined. C₃₁17 β ,21 β (H) hopane was
14 the dominant hopane. No $\alpha\beta$ -hopanes were encountered, so the ($\beta\beta/(\beta\beta+\beta\alpha+\alpha\alpha)$) of hopane
15 biomarkers was 1. This is in perfect agreement with Blumenberg and Wiese (2012), who
16 report that various types of hopanoids, for the same core, are dominated by the 17 β , 21 β (H)-
17 stereochemistry. This indicates that the thermal maturity of the sedimentary organic matter
18 was sufficiently low for the application of TEX₈₆ paleothermometry (cf. Schouten et al.,
19 2004).

20 Blumenberg and Wiese (2012) also report much higher degrees of thermal maturity based
21 upon isomerization ratios of biomarkers in hydropyrolysates generated from the kerogen.
22 However, to obtain these pyrolysates, kerogens were heated by temperatures up to 500°C. It is
23 well known that during such experiments the degree of isomerization of biomarkers alters
24 towards a thermodynamic equilibrium mixture depending on time of the experiment and
25 temperature applied (e.g., Koopmans et al., 1996). Accordingly, the data of Blumenberg and
26 Wiese (2012) obtained from the hydropyrolysates are not relevant to assess the natural level
27 of thermal maturity. Therefore there is no conflict between the data of Blumenberg and Wiese
28 (2012) and the data presented in this study.

29 **3.3 GDGT-based proxies**

30 Except for Sample 41.45 mbs, all samples yielded quantifiable GDGT abundances, although
31 with orders of magnitude differences in concentration (Fig. 2c). Total GDGT concentrations
32 are in the range of 0.13-43 $\mu\text{g/g}$ organic carbon (OC). Crenarchaeol concentrations vary by
33 three orders of magnitude, whereas brGDGT concentrations vary by one to two orders of
34 magnitude. High GDGT concentrations coincide with the organic carbon-rich black shales

1 (Figs. 2b,c), while low GDGT concentrations coincide with organic-poor sediments (Figs.
2 2b,c). Values for the BIT-index range from 0.02, indicating low relative abundances of soil-
3 derived brGDGTs, to 0.56, evidencing substantial soil-derived input of brGDGTs. The BIT-
4 index (Fig. 2d) is relatively high in the organic-poor intervals and generally low (i.e. <0.10)
5 for the organic-rich black-shale intervals. Values for TEX₈₆ fluctuate between 0.71 and 0.99
6 (Fig. 2e).

7

8 **3.4 Palynology**

9 Nine samples were barren of palynomorphs (Fig. 3c). For the remaining 42 samples, dinocyst
10 concentrations range from ~35 to 15000 cysts per gram, and pollen and spores concentrations
11 range from 10> to 5000 grains per gram, with highest concentrations in the organic-rich black
12 shales (Fig. 3c).

13 Palynological assemblages are dominated by dinocysts, ~85% on average (max. >99%).
14 Summed pollen and spores, and hence the terrestrially derived fraction, comprises on average
15 ~15% of the assemblage (max. ~40%). The terrestrial over marine palynomorph ratio (T/M-
16 ratio) was calculated by dividing terrestrial palynomorphs (pollen and spores) by aquatic
17 palynomorphs (dinocysts and acritarchs). In general T/M-values are elevated in the organic-
18 rich intervals (Fig. 3h), while minima in the T/M-ratio correspond to organic-poor intervals.

19 Age-diagnostic dinocyst species include *Lithosphaeridium siphoniphorum siphoniphorum*, a
20 marker species for the CTB interval in the northwest European reference section at
21 Eastbourne (Pearce et al., 2009). The last occurrence of *L.siphoniphorum siphoniphorum* is at
22 47.81 mbs (Fig. 3f), confirming a latest Cenomanian age.

23 Dinocyst assemblages are dominated by multiple species of the Peridiniaceae family, i.e.,
24 *Paleohystrichophora infusorioides*, *Subtilisphaera pontis-mariae*, *Eurydinium saxoniense*,
25 *Isabelidinium* spp., and *Ginginodinium* spp.. Members of this family have repeatedly been
26 shown to be derived of low-salinity tolerant dinoflagellates in Late Cretaceous and Paleogene
27 successions and likely represent heterotrophic, euryhaline dinoflagellates (e.g., Harland, 1973;
28 Sluijs and Brinkhuis, 2009; Powell et al., 1990; Lewis et al., 1990; Fig. 3c). Other
29 quantitatively important taxa include *Spiniferites* spp. (Fig.3d) and *Impagidinium* spp. (Fig.
30 3e), which are generally associated with outer shelf to oceanic environments (e.g., Wall et al.,
31 1977; Harland, 1983; Brinkhuis, 1994). Commonly present are representatives of
32 *Odontochitina*, *Oligosphaeridium*, *Exochosphaeridium*, *Downiesphaeridium*,
33 *Cyclonephelium*, *Lithosphaeridium*, *Achomosphaera*, and *Florentinia* spp., which are, like

1 most encountered pollen and spores, typical for Late Cretaceous dinocyst shelf to bathyal
2 assemblages (e.g., Dodsworth, 2004; Pearce et al., 2009; Peyrot et al., 2012).

3 4 **4. Discussion**

5 **4.1 SST reconstruction**

6 **4.1.1 Input of terrestrially derived GDGTs and post-depositional oxidation**

7 Small quantities of iGDGTs as used for determination of TEX₈₆ values, are also produced in
8 soils. High input of soil-derived iGDGTs, reflected by elevated BIT index values, might
9 therefore bias TEX₈₆-derived SST reconstructions (Weijers et al., 2006). TEX₈₆ and BIT
10 index values for the OAE2-record of the Wunstorf core exhibit a negative linear relation (R^2 -
11 value of 0.43; Fig. 4), which may be the result of relatively high input of soil-derived
12 iGDGTs, potentially affecting TEX₈₆ values. Previous work has recommended a cut-off value
13 of the BIT index to exclude this effect from TEX₈₆-based paleotemperature reconstructions
14 (Weijers et al., 2006).

15 Low-TOC sediments have high BIT index values and low TOC-normalized concentrations for
16 brGDGTs and, to a larger extent, iGDGTs (Fig. 5). This is similar to results from TOC-rich
17 turbidites that are affected by post-depositional oxidation (e.g., Huguet et al., 2008; Lengger
18 et al., 2013). This was explained by preferential preservation of soil-derived brGDGTs over
19 marine-derived iGDGTs upon post-depositional oxidation of the turbidites. For the Wunstorf
20 section, the marls and limestones represent depositional phases during which the water
21 column and pore waters of surface sediments contained relatively high concentrations of
22 oxygen, as is evident from bioturbation, low TOC content (Fig. 2b), and low levels of redox-
23 sensitive trace elements (Hetzl et al., 2011). Diagenetic effects caused by the oxidation of
24 biomarkers in the water column and pore waters most likely played a substantial role in this
25 depositional setting. Preferential preservation of brGDGTs is therefore likely responsible for
26 the observed pattern in the BIT-index. Although Lengger et al. (2013) did not find a bias in
27 TEX₈₆ values for sediments that suffered post-depositional oxidation, other studies have
28 shown that there can be a considerable post-depositional oxidation effect on TEX₈₆ values and
29 thus the paleo-SST reconstructions derived from it (e.g., Huguet et al., 2009). The linear
30 correlation between TEX₈₆ and BIT-index values for the analyzed sediments of the Wunstorf
31 core, is in line with the latter.

32 Based on the relation between TOC and the BIT-index (Fig. 5a) and the concentrations of the
33 sum of the brGDGTs and crenarcheol (Fig. 5b), we decided to remove reconstructed paleo-
34 SST data with a BIT-index > 0.15. This changes the linear correlation between TEX₈₆ and

1 BIT-index, suggesting that samples with a BIT-index > 0.15 are affected by post-depositional
2 oxidation. This results in a dataset in which samples with a BIT-index value between 0.02 and
3 0.12 are considered for paleo-SST reconstructions, removing the impact of soil derived
4 iGDGTs on the paleo-SST reconstructions.

6 **4.1.2 Trends, stratigraphic correlation and absolute values**

7 Trends and values of the reconstructed SSTs at Wunstorf using the $\text{TEX}_{86}^{\text{H}}$ -calibration of Kim
8 et al. (2010; Fig. 6c) are similar to previous TEX_{86} -based SST reconstructions for OAE2.
9 Previously studied sites were located in the equatorial Atlantic (DSDP Site 367 and ODP Site
10 1260; Forster et al., 2007) and the mid-latitudes (ODP Site 1276 – Sinninghe Damsté et al.,
11 2010; Bass River – van Helmond et al., 2014; Fig. 1). Potentially due to a lack of reliable
12 TEX_{86} values at the onset of the OAE2-interval (Fig. 6b), the Wunstorf SST record does not
13 capture the rapid increase in SST at the onset of OAE2, previously attributed to a rise in
14 atmospheric CO_2 released by extensive volcanism (e.g., Forster et al., 2007). The Wunstorf
15 SST-record does show, despite being supported by predominantly one data point (resulting
16 from the removal of samples with a BIT-index > 0.15), a $\sim 5^\circ\text{C}$ cooling pulse during the early
17 stages of OAE2 (Fig. 6c). Six consecutive samples following our data point with lowest SST
18 support a subsequent warming trend, following a colder phase, however.

19 Based on its stratigraphic position within the early stages of the CIE, we attribute this cooling
20 pulse to the Plenus Cold Event (PCE; Gale and Christensen, 1996). The PCE, an event first
21 recognized as an incursion of boreal fauna in the shelf seas of NW Europe (e.g., Jefferies,
22 1962; Gale and Christensen, 1996; Voigt et al., 2004), represents a substantial cooling event
23 based on TEX_{86} -based paleo-SST records throughout the proto-North Atlantic basin (Forster
24 et al., 2007; Sinninghe Damsté et al., 2010; van Helmond et al., 2014). At Wunstorf the data
25 point with lowest SST correlates to a level above the Plenusbank, located at 47.30–46.85 mbs
26 (Voigt et al., 2008) after the maximum in the CIE. The lack of reliable SST data for the
27 interval between 47.74 and 46.21 mbs complicates precise determination of the onset of the
28 PCE at Wunstorf, however. In three more “complete”, previously published TEX_{86} -based
29 paleo-SST records across the PCE, i.e., ODP Site 1260 (Forster et al., 2007), ODP Site 1276
30 (Sinninghe Damsté et al., 2010) and Bass River (van Helmond et al., 2014) the cooling in
31 TEX_{86} -based SSTs starts before the first maximum in the CIE, prior to the occurrence of
32 boreal fauna in the shelf seas of NW Europe (Gale and Christensen, 1996), suggesting that
33 faunal migrations lagged the cooling event as reconstructed by TEX_{86} . Therefore precise
34 correlations of the PCE between sites remains challenging. The identification of the PCE at

1 Wunstorf, alongside the previous identifications of the PCE throughout the proto-North
2 Atlantic basin, suggest that the PCE was a hemisphere-wide and perhaps even a global event.
3 This supports the hypothesis that enhanced global carbon burial temporarily suppressed
4 atmospheric CO₂ levels during OAE2 (Arthur et al., 1988; Sinninghe Damsté et al., 2010).
5 The PCE is related to changes in ocean circulation, recorded by the incursion of a northerly
6 sourced water mass as derived from a negative neodymium isotope excursion in the English
7 Chalk at Eastbourne (Zheng et al., 2013) and a trace-metal anomaly in the Western Interior
8 Seaway (Eldrett et al., 2014). This northerly sourced water mass may have been instrumental
9 for the dispersion of boreal fauna in the shelf seas of NW Europe, in line with the observed
10 differences in timing between TEX₈₆-based cooling in SSTs and the occurrence of boreal
11 fauna. Interestingly, the interval of the PCE marks the occurrence of the *Cyclonephelium*
12 *compactum-membraniphorum* complex (*C. comp.-memb. cplx.*) within the OAE2 interval in
13 the Wunstorf core (Fig. 6c,d). This is in accordance with previous records from the Bass
14 River section (van Helmond et al., 2014) and the Shell Iona-1 core (Eldrett et al., 2014).
15 Although the biogeographic distribution of this complex is still partly unclear, this suggests
16 that the introduction of *C. comp.-memb. cplx.* at mid-latitude sites in both northwest Europe
17 and the east coast of North-America was quasi-instantaneous and linked to the PCE.
18 No significant difference in the reconstructed SSTs is recorded between the black shales and
19 the more TOC-lean marls and limestones. This suggests that the cyclic deposition of black
20 shales during OAE2 in the LSB was not primarily driven by changes in SST.
21 Average SSTs for the OAE2-interval at Wunstorf are higher than at Bass River (New Jersey
22 Shelf), DSDP Site 367 (Cape Verde Basin), ODP Site 1260 (Demarara Rise), and Site 1276
23 (North Atlantic; Table 1), which may perhaps be an artefact of the low resolution achieved for
24 the Plenus Cold Event at Wunstorf. Reconstructions of absolute temperatures based on TEX₈₆
25 at values significantly exceeding the modern calibration may yield significant errors, since the
26 modern core-top calibration only ranges to 30°C (Kim et al., 2010). Therefore SSTs
27 exceeding this value will always be based on extrapolation, although mesocosm studies have
28 revealed that TEX₈₆ also shows a positive response with increasing temperatures, in the 30-
29 40°C range (Schouten et al., 2007b). Furthermore the logarithmic TEX₈₆^H-index (Kim et al.,
30 2010), used in this study, has a calibration maximum of 38.6°C, i.e., when TEX₈₆ = 1 the
31 reconstructed SST is 38.6°C. SSTs reconstructions for samples with a TEX₈₆-value >0.9 may
32 therefore be relatively conservative. Nonetheless, the warm and relatively stable background
33 SSTs for Wunstorf (~37°C) suggest that SSTs on the European shelf were exceptionally high

1 and supports the notion that thermal gradients were substantially reduced during the Late
2 Cretaceous greenhouse world (e.g., Baron, 1983; Huber et al., 1995).

3 4 **4.2 Hydrology**

5 Although pollen rank among the most resistant groups of palynomorphs (Traverse, 1994),
6 there is evidence that pollen grains are degraded relatively rapidly (<10 kyr) in the presence
7 of diffusively introduced oxygen (e.g., Keil et al., 1994). This may perhaps explain why
8 absolute pollen and spores concentrations are higher in the black shales, deposited under
9 anoxic conditions. This contrasts with the organic lean marls and limestones deposited during
10 phases in which pore waters of surface sediments contained relatively high concentrations of
11 oxygen, explaining the low absolute pollen and spores concentrations.

12 Among modern dinoflagellate cysts, members of the family Protoperidiniaceae, are most
13 sensitive to oxidation, and thus may potentially be affected by differential preservation (e.g.,
14 Zonneveld, et al., 1997, Zonneveld et al., 2001; Versteegh and Zonneveld, 2002). No
15 consensus exists in the field whether this differential preservation is imprinted in the
16 sedimentary record (e.g., Reichart and Brinkhuis, 2003). At present, there is no published
17 information that suggests that the selective preservation of dinocysts plays a role in
18 assemblages described from the Cretaceous. If there were one dinocyst taxon potentially
19 prone to be selectively degraded in the assemblages we record, it would be the thin-walled
20 taxon *Paleohystrichophora infusorioides*, which also belongs to the peridinioids. Well-
21 preserved representatives of *P. hystrichophora* are, however, commonly present in the organic
22 lean marls and limestones.

23 Pollen and spores are transported to the marine environment by a wide range of processes,
24 with river discharge and wind being the most important factors (e.g., Traverse and Ginsburg,
25 1966; Thomson, 1986; Feinsinger and Busby, 1987). Particularly saccate gymnosperm pollen
26 (bisaccates) may be transported by eolian pathways (e.g., Heusser, 1988). Palynological
27 assemblages at Wunstorf are a mixture of saccate gymnosperm pollen and non-saccate
28 gymnosperm pollen and spores, suggesting a mixture of eolian and fluvial input of pollen and
29 spores. However, most of the analyzed samples contain relatively low amounts of saccate
30 gymnosperm pollen (Fig. 6e; Prauss, 2006), suggesting that a substantial amount of the pollen
31 and spores encountered at Wunstorf was transported to the marine realm by fluvial processes.
32 The relatively high amounts of pollen and spores with respect to marine palynomorphs (T/M-
33 ratio; Fig. 6e) in the black shales at Wunstorf are therefore interpreted to represent phases of
34 enhanced run-off. This was previously also shown for other Cretaceous Oceanic Anoxic

1 Events (e.g., Herrle et al., 2003). Enhanced run-off most likely resulted from increased
2 (seasonal) precipitation over north and mid-European landmasses, assuming that these yielded
3 significant vegetation cover. Regarding the distance to the coring site, non-saccate pollen and
4 spores most likely originated from the Rheno-Bohemian Massif (e.g., Falcon-Lang et al.,
5 2001; Herman et al., 2002), which is in accordance with the prevailing paleo-wind directions
6 (Hay and Floegel, 2012). Enhanced (seasonal) influx of fresh, low-density, surface waters
7 could well have stratified the water column, leading to low-oxygen levels in bottom waters.
8 This is also indicated by high abundances of bacterivorous ciliates (Blumenberg and Wiese,
9 2012), which graze on the interfaces of stratified water bodies (Sinninghe Damsté et al.,
10 1995), supporting the presence of a chemocline in the water column. A persistent
11 stratification of the water column ultimately leads to bottom water anoxia and the formation
12 of black shales in the deeper parts of the LSB. The coupling of the rhythmical occurrence of
13 the black shale layers to the precession cycle (Voigt et al., 2008) suggests that changes in the
14 hydrological cycle were controlled by Earth's orbital parameters.

15

16 **4.3 Marine Productivity**

17 High abundances of dinocysts and organic matter in general may result from both enhanced
18 marine primary productivity and an improved preservation potential for organic matter during
19 black shale deposition. In modern oceans, most peridinioid dinocysts are produced by
20 heterotrophic dinoflagellates, whilst most gonyaulacoid dinocysts are derived from
21 autotrophic taxa (Lewis et al., 1990). As a consequence, the ratio between peridinioids and
22 gonyaulacoids (P/G-ratio) has been employed widely as a proxy for paleoproductivity (Sluijs
23 et al., 2005). In the Wunstorf OAE2-section, the P/G-ratio reaches maximum values within
24 the different black shale couplets, implying that productivity was elevated during their
25 deposition (Fig. 6f). Furthermore the peridinioids encountered at Wunstorf belong to the
26 Peridiniaceae family, which has been shown to be low-salinity tolerant (e.g., Harland, 1973;
27 Sluijs and Brinkhuis, 2009). Together, this suggests that during seasons of high precipitation
28 and run-off that introduced nutrients a low-salinity, high-productivity surface layer existed in
29 the Lower Saxony Basin. This hypothesis is supported by assemblages of calcareous
30 nannofossils, showing a shift from a generally oligotrophic ecosystem to more mesotrophic or
31 even eutrophic conditions during black shale deposition (Linnert et al., 2010).

32 Enhanced marine primary productivity likely contributed to the establishment of bottom water
33 anoxia by increasing the flux of organic matter to the seafloor, depleting bottom water oxygen
34 concentrations upon decay.

1
2
3
4
5
6
7
8
9
10
11
12
13
14
15
16
17
18
19
20
21
22
23
24
25
26
27
28
29
30
31
32
33
34

5. Conclusions

Despite differences in the preservation of organic matter throughout the OAE2 interval at Wunstorf, the general trend in reconstructed SSTs, including the cooling phase associated with the Plenus Cold Event, is consistent with the results of previous studies that targeted the proto-North Atlantic. Hence, the SST trend recorded at Wunstorf and the other sites was of at least hemispheric significance. Reconstructed SSTs do not substantially differ between black shales and less organic-rich deposits. This implies that, although higher temperatures must have had an effect on the solubility of oxygen in seawater, surface temperature was not the critical factor for the cyclic deposition of organic matter. Absolute SSTs for the Wunstorf OAE2 section show little or no difference in comparison with SST reconstructions for sites located at lower latitudes, which were evaluated using the same proxy and the same methodology. This confirms that thermal gradients were much reduced during the Late Cretaceous (Barron, 1983; Huber et al., 1995).

The dinocyst complex *Cyclonephelium compactum*–*C. membraniphorum*, previously linked to the Plenus Cold Event (van Helmond et al., 2014), was encountered at the respective level at Wunstorf, suggesting that its occurrence is indeed linked to this cooling. Its continued presence in the remainder of the record suggests, however, that other paleoenvironmental factors were also critical in controlling its distribution.

A combination of continental configuration and extensive volcanism, intensifying greenhouse conditions around the CTB, resulted in an epicontinental shelf sea prone to black shale deposition as a consequence of precession-driven climate change at Wunstorf, (Voigt et al., 2008). We conclude, based on relatively high numbers of terrestrially derived pollen and spores and freshwater tolerating dinocysts in the black shale intervals, that precession was driving variations in the hydrological cycle. This caused (seasonal) freshwater stratification of the water column and likely enhanced primary production, ultimately culminating in bottom water anoxia and black shale formation. An orbitally controlled hydrological cycle may have been a critical factor for other cyclic OAE2 sites located in the proto-Atlantic and Western Interior Seaway at similar latitudes as well.

Acknowledgements

The Wunstorf Coring Scientific Drilling Party is thanked for providing the chance to work on their exceptionally well-recovered core. We thank Itzel Ruvalcaba Baroni and Walter Hale for sampling support, and Dominika Kasjaniuk, Arnold van Dijk, Natasja Welters, Jan van

1 Tongeren (Utrecht University), and Anhelique Mets (NIOZ) for analytical assistance and
2 sample preparation. Andrew Gale and David Naafs are thanked for their constructive reviews.
3 We acknowledge NWO for funding the purchase of the HPLC-MS (grant no. 834.11.006)
4 used for the GDGT analyses presented in this study. This research was supported by the
5 ‘Focus & Massa project’ of Utrecht University granted to Henk Brinkhuis and Caroline
6 Slomp, and additional financial support by Statoil. The European Research Council (ERC)
7 under the European Union Seventh Framework Program provided funding for this work by
8 ERC Starting Grant #259627 to Appy Sluijs.

9

10 **References**

- 11 Arthur, M.A., Dean, W.E., and Pratt, L.M.: Geochemical and climatic effects of increased
12 marine organic carbon burial at the Cenomanian/Turonian boundary, *Nature*, 335, 714–717,
13 doi:10.1038/335714a0, 1988.
- 14 Barclay, R.S., McElwain, J.C., and Sageman, B.B.: Carbon sequestration activated by
15 a volcanic CO₂ pulse during Oceanic Anoxic Event 2, *Nat. Geosci.*, 3, 205–208,
16 doi:10.1038/NGEO757, 2010.
- 17 Barron, E.J.: A warm, equable Cretaceous: the nature of the problem, *Earth-Sci. Rev.*, 19(4),
18 305–338, doi:10.1016/0012-8252(83)90001-6, 1983.
- 19 Blättler, C.L., Jenkyns, H.C., Reynard, L.M., and Henderson, G.M. : Significant increases in
20 global weathering during Oceanic Anoxic Events 1a and 2 indicated by calcium isotopes,
21 *Earth Planet. Sc. Lett.*, 309, 77–88, doi:10.1016/j.epsl.2011.06.029, 2011.
- 22 Blumenberg, M., and Wiese, F.: Imbalanced nutrients as triggers for black shale formation in a
23 shallow shelf setting during the OAE 2 (Wunstorf, Germany), *Biogeosciences*, 9, 4139–4153,
24 doi:10.5194/bg-9-4139-2012, 2012.
- 25 Bice, K.L., Birgel, D., Meyers, P.A., Dahl, K.A., Hinrichs, K.-U., and Norris, R.D.: A
26 multiple proxy and model study of the Cretaceous upper ocean temperatures and atmospheric
27 CO₂ concentrations, *Paleoceanography*, 21, PA2002, doi:10.1029/2005PA001203, 2006.
- 28 Brinkhuis, H.: Late Eocene to Early Oligocene dinoflagellate cysts from the Priabonian type-
29 area (northeast Italy): biostratigraphy and palaeoenvironmental interpretation.
30 *Palaeogeogr. Palaeoclimatol.*, 107, 121–163, doi:10.1016/0031-0182(94)90168-6, 1994.
- 31 Creaney, S., and Passey, Q.R.: Recurring Patterns of Total Organic Carbon and Source Rock
32 Quality within a Sequence Stratigraphic Framework, *AAPG Bull.* 77, 386–401, 1993.

1 Dodsworth, P.: The palynology of the Cenomanian–Turonian (Cretaceous) boundary
2 succession at Aksudere in Crimea, Ukraine, *Palynology*, 28, 129–141, doi:10.2113/28.1.129,
3 2004.

4 Du Vivier, A.D.C., Selby, D., Sageman, B.B., Jarvis, I., Gröcke, D.R., and Voigt, S.: Marine
5 $^{187}\text{Os}/^{188}\text{Os}$ isotope stratigraphy reveals the interaction of volcanism and ocean circulation
6 during Oceanic Anoxic Event 2, *Earth Planet. Sc. Lett.*, 389, 23–33,
7 doi:10.1016/j.epsl.2013.12.024, 2014.

8 Eldrett, J.S., Minisini, D., and Bergman, S.C.: Decoupling of the carbon cycle during Ocean
9 Anoxic Event 2. *Geology* 42, 567-570, doi:10.1130/G35520.1, 2014.

10 Erbacher, J., Thurow, J., and Littke, R.: Evolution patterns of radiolarian and organic matter
11 variations: A new approach to identify sea-level changes in mid-Cretaceous pelagic
12 environments, *Geology*, 6, 499–502. doi:10.1130/0091-7613, 1996.

13 Erbacher, J., Mutterlose, J., Wilmsen, M., Wonik, T., and Party, W. D. S.: The Wunstorff
14 Drilling Project: Coring a global stratigraphic reference section of the Oceanic Anoxic Event
15 2, *Scientific Drilling*, 4, 19–21, 2007.

16 Ernst, G., Wood, C.J., and Hilbrecht, H.: The Cenomanian-Turonian boundary problem in
17 NW-Germany with comments on the north-south correlation to the Regensburg area, *Bull.*
18 *Geol. Soc. Den.*, 33, 103–113, 1984.

19 Falcon-Lang, H.J., Kvacek, J., and Ulicný, D.: Fire-prone plant communities and
20 palaeoclimate of a Late Cretaceous fluvial to estuarine environment, Pecínov quarry, Czech
21 Republic. *Geological Magazine*, 138, 563-576, 2001.

22 Feinsinger, P., and Busby, W.H.: Pollen carryover: experimental comparisons between
23 morphs of *Palicourea lasiorrachis* (Rubiaceae), a distylous, bird-pollinated, tropical treelet,
24 *Oecologia*, 73(2), 231-235, 1987

25 Fensome, R.A., and Williams, G.L.: The Lentin and Williams Index of Fossil Dinoflagellates,
26 2004 Edition, American Association of Stratigraphic Palynologists Contribution Series 42,
27 909 pp, 2004.

28 Forster, A., Schouten, S., Moriya, K., Wilson, P.A., and Sinninghe Damsté, J.S.: Tropical
29 warming and intermittent cooling during the Cenomanian/Turonian Oceanic Anoxic Event
30 (OAE 2): Sea surface temperature records from the equatorial Atlantic, *Paleoceanography*, 22,
31 PA1219. doi:10.1029/2006PA001349, 2007.

32 Forster, A., Kuypers, M.M.M., Turgeon, S.C., Brumsack, H.-J., Petrizzo, M.R., Sinninghe
33 Damsté, J.S.: The Cenomanian/Turonian oceanic anoxic event in the South

1 Atlantic: new insights from a geochemical study of DSDP Site 530A, *Palaeogeogr. Palaeocl.*,
2 267, 256–283, doi:10.1016/j.palaeo.2008.07.006, 2008.

3 Gale, A.S., and Christensen, W.K.: Occurrence of the belemnite *Actinocamax plenus* in the
4 Cenomanian of SE France and its significance, *Bull. Geol. Soc. Den.*, 43, 68–77, 1996.

5 Hancock, J.M., and Kauffman, E.G.: The great transgressions of the Late Cretaceous. *J. Geol.*
6 *Soc. London*, 136, 175–186, 1979.

7 Harland, R.: Dinoflagellate cysts and acritarchs from the Bearpaw Formation (Upper
8 Campanian) of southern Alberta, Canada, *Palaeontology*, 16, 665-706, 1973.

9 Harland, R.: Distribution maps of recent dinoflagellate cysts in bottom sediments from the
10 North Atlantic Ocean and adjacent seas, *Palaeontology*, 26, 321-387, 1983.

11 Hay, W.W., and Flögel, S.: New thoughts about the Cretaceous climate and oceans, *Earth-Sci.*
12 *Rev.*, 115(4), 262-272, doi:10.1016/j.earscirev.2012.09.008, 2012.

13 Herman, A.B., Spicer, R.A., and Kvaček, J.: Late Cretaceous climate of Eurasia and Alaska: a
14 quantitative palaeobotanical approach, in: *Aspect of Cretaceous Stratigraphy and*
15 *Palaeobiogeography*, edited by: Wagreich, M., *Österreichische Akademie der Wissenschaften*, 15.
16 93–108, 2002.

17 Herrle, J. O., Pross, J., Friedrich, O., Kößler, P., and Hemleben, C.: Forcing mechanisms for
18 mid-Cretaceous black shale formation: evidence from the Upper Aptian and Lower Albian of
19 the Vocontian Basin (SE France), *Palaeogeogr. Palaeocl.*, 190, 399-426, 2003.

20 Hetzel, A., März, C., Vogt, C., and Brumsack, H.-J.: Geochemical environment of
21 Cenomanian–Turonian black shale deposition at Wunstorf (northern Germany), *Cretaceous*
22 *Res.*, 32, 480–494, doi:10.1016/j.cretres.2011.03.004, 2011.

23 Heusser, L.E.: Pollen distribution in marine sediments on the continental margin off northern
24 California, *Mar. Geol.*, 80, 131–147, 1988.

25 Hopmans, E.C., Weijers, J.W.H., Schefuß, E., Herfort, L., Sinninghe Damsté, J.S., and
26 Schouten, S.: A novel proxy for terrestrial organic matter in sediments based on branched and
27 isoprenoid tetraether lipids, *Earth Planet. Sc. Lett.*, 224, 107–116,
28 doi:10.1016/j.epsl.2004.05.012, 2004.

29 Huber, B.T., Hodell, D.A., and Hamilton, C.P.: Middle–Late Cretaceous climate of the
30 southern high latitudes: stable isotopic evidence for minimal equator-to-pole thermal
31 gradients, *Geol. Soc. Am. Bull.*, 107, 1164–1191, doi:10.1130/0016-
32 7606(1995)107<1164:MLCCOT>2.3.CO;2, 1995.

33 Huguet, C., Hopmans, E. C., Febo-Ayala, W., Thompson, D. H., Sinninghe Damsté, J. S., and
34 Schouten, S.: An improved method to determine the absolute abundance of glycerol di

1 biphytanyl glycerol tetraether lipids, *Org. Geochem.*, 37, 1036-1041,
2 doi:10.1016/j.orggeochem.2006.05.008, 2006.

3 Huguet, C., de Lange, G.J., Middelburg, J.J., Sinninghe Damsté, J.S., and Schouten,
4 S.: Selective preservation of soil organic matter in oxidized marine sediments (Madeira
5 Abyssal Plain), *Geochim. Cosmochim. Ac.*, 72, 6061–6068, doi:10.1016/j.gca.2008.09.021,
6 2008.

7 Huguet, C., Kim, J.-H., de Lange, G.J., Sinninghe Damsté, J.S., and Schouten, S.: Effects of
8 long-term oxic degradation on the $U^{K'}_{37}$, TEX₈₆ and BIT organic proxies, *Org. Geochem.*, 40,
9 1188–1194, doi:10.1016/j.orggeochem.2009.09.003, 2009.

10 Jarvis, I., Lignum, J.S., Gröcke, D.R., Jenkyns, H.C., and Pearce, M.A.: Black shale
11 deposition, atmospheric CO₂ drawdown, and cooling during the Cenomanian-Turonian
12 Oceanic Anoxic Event: *Paleoceanography* 26, PA3201. doi:10.1029/2010PA002081, 2011.

13 Jefferies, R.P.S.: The palaeoecology of the *Actinocamax plenus* subzone (lowest Turonian) in
14 the Anglo-Paris Basin, *Palaeontology*, 4, 609–647, 1962.

15 Jenkyns, H.C.: Geochemistry of oceanic anoxic events, *Geochem. Geophys. Geosy.*, 11,
16 Q03004. doi:10.1029/2009GC002788, 2010.

17 Junium, C.K., and Arthur, M.A.: Nitrogen cycling during the Cretaceous, Cenomanian-
18 Turonian Oceanic Anoxic Event II. *Geochem. Geophys. Geosy.*, 8, Q03002.
19 doi:10.1029/2006GC001328, 2007.

20 Keil, R.G., Hu, E.S., Tsamakis, E.C., and Hedges, J.I.: Pollen in marine sediments as an
21 indicator of oxidation of organic matter, *Nature*, 369, 639-641, doi:10.1038/369639a0, 1994.

22 Kerr, A.C.: Oceanic plateau formation: a cause of mass extinction and black shale deposition
23 around the Cenomanian–Turonian boundary?, *J. Geol. Soc. London*, 155, 619–626, doi:
24 10.1144/gsjgs.155.4.0619, 1998.

25 Kim, J.-H., van der Meer, J., Schouten, S., Helmke, P., Willmott, V., Sangiorgi, F., Koç, N.,
26 Hopmans, E.C., and Sinninghe Damsté, J.S.: New indices and calibrations derived from the
27 distribution of crenarchaeal isoprenoid tetraether lipids: Implications for past sea surface
28 temperature reconstructions, *Geochim. Cosmochim. Ac.*, 74, 4639–4654,
29 doi:10.1016/j.gca.2010.05.027, 2010.

30 Koopmans, M.P., De Leeuw, J.W., Lewan, M.D., and Sinninghe Damsté, J.S.: Impact of dia-
31 and catagenesis on sulphur and oxygen sequestration of biomarkers as revealed by artificial
32 maturation of an immature sedimentary rock, *Organic Geochemistry*, 25, 391-426, 1996.

1 Kuroda, J., Ogawa, N., Tanimizu, M., Coffin, M., Tokuyama, H., Kitazato, H., and Ohkouchi,
2 N.: Contemporaneous massive subaerial volcanism and late cretaceous Oceanic Anoxic Event
3 2, *Earth Planet. Sc. Lett.*, 256, 211–223, doi:10.1016/j.epsl.2007.01.027, 2007.

4 Kuypers, M.M.M., Lourens, L.J., Rijkstra, W.I.C., Pancost, R.D., Nijenhuis, I.A., and
5 Sinninghe Damsté, J.S.: Orbital forcing of organic carbon burial in the proto-North Atlantic
6 during oceanic anoxic event 2, *Earth Planet. Sc. Lett.* 228, 465–482,
7 doi:10.1016/j.epsl.2004.09.037, 2004a.

8 Kuypers, M.M.M., van Breugel, Y., Schouten, S., Erba, E., and Sinninghe Damsté, J.S.: N₂-
9 fixing cyanobacteria supplied nutrient N for Cretaceous oceanic anoxic events, *Geology*, 32,
10 853–856. doi:10.1130/G20458.1, 2004b.

11 Lengger, S.K., Kraaij, M., Tjallingii, R., Baas, M., Stuut, J.B., Hopmans, E.C., Sinninghe
12 Damsté, J.S., and Schouten, S.: Differential degradation of intact polar and core glycerol
13 dialkyl glycerol tetraether lipids upon post-depositional oxidation, *Org. Geochem.*, 65, 83-93,
14 doi:10.1016/j.orggeochem.2013.10.004, 2013.

15 Lewis, J., Dodge J.D., and Powell, J.: Quaternary dinoflagellate cysts from the upwelling
16 system offshore Peru, Hole 686B, ODP Leg 112, in: *Proceedings of the Ocean Drilling
17 Program, Scientific Results*, edited by: Suess, E., Von Huene, R., et al., 112, 323-328, 1990.

18 Linnert, C., Mutterlose, J., and Erbacher, J.: Calcareous nannofossils of the
19 Cenomanian/Turonian boundary interval from the Boreal Realm (Wunstorf, northwest
20 Germany), *Mar. Micropaleontol.*, 74, 38–58, doi:10.1016/j.marmicro.2009.12.002, 2010.

21 Marshall, K.L., and Batten, D.J.: Dinoflagellate cyst associations in Cenomanian–Turonian
22 “black shale” sequences of northern Europe, *Rev. Palaeobot. Palyno.*, 54, 85–103, 1988.

23 Meyers, S.R., Sageman, B.B., and Arthur, M.A.: Obliquity forcing and the amplification of
24 high-latitude climate processes during Oceanic Anoxic Event 2, *Paleoceanography*, 27,
25 PA3212, doi:10.1029/2012PA002286, 2012.

26 Miller, K.G., Kominz, M.A., Browning, J.V., Wright, J.D., Mountain, G.S., Katz, M.E.,
27 Sugarman, P.J., Carter, B.S., Christie-Blick, N., and Pekar, S.F.: The Phanerozoic record of
28 global sea-level change, *Science*, 310, 1293–1298. doi:10.1126/science.1116412, 2005.

29 Mort, H.P., Adatte, T., Föllmi, K.B., Keller, G., Steinmann, P., Matera, V., Berner, Z.,
30 Stuben, D.: Phosphorus and the roles of productivity and nutrient recycling during oceanic
31 anoxic event 2, *Geology*, 35, 483–486, doi:10.1130/G23475A.1, 2007.

32 Pearce, M.A., Jarvis, I., and Tocher, B.A.: The Cenomanian-Turonian boundary event, OAE 2
33 and palaeoenvironmental change in epicontinental seas: new insights from the dinocyst and

1 geochemical records, *Palaeogeograph. Palaeocl.*, 280, 207-234, doi:
2 10.1016/j.palaeo.2009.06.012, 2009.

3 Peyrot, D., Barroso-Barcenilla, F., and Feist-Burkhardt, S.: Palaeoenvironmental controls on
4 late Cenomanian–early Turonian dinoflagellate cyst assemblages from Condemios (Central
5 Spain), *Rev. Palaeobot. Palyno.*, 180, 25–40, doi:10.1016/j.revpalbo.2012.04.008, 2012.

6 Pogge von Strandmann, P.A.E., Jenkyns, H.C., and Woodfine, R.G.: Lithium isotope
7 evidence for enhanced weathering during Oceanic AnoxicEvent 2, *Nat. Geosci.*, 6, 668–672,
8 doi:10.1038/ngeo1875, 2013.

9 Poulsen, J. C., Barron, E.J., Arthur, A., and Peterson, H.: Response of the mid-Cretaceous
10 global oceanic circulation to tectonic and CO₂ forcings, *Paleoceanography*, 16, 576–592,
11 doi:10.1029/2000PA000579, 2001.

12 Powell, A.J., Dodge, J.D., Lewis, J.: Late Neogene to Pleistocene palynological facies of the
13 Peruvian continental margin upwelling, Leg 112, in: *Proceedings of the Ocean Drilling
14 Program, Scientific Results*, edited by: Suess, E., Von Huene, R., et al., 112, 297-321, 1990.

15 Prauss, M.L.: The Cenomanian–Turonian Boundary Event (CTBE) at Wunstorf, north-west
16 Germany, as reflected by marine palynology, *Cretaceous Res.*, 27, 872–886,
17 doi:10.1016/j.cretres.2006.04.004, 2006.

18 Reichart, G.J., Brinkhuis, H.: Late Quaternary *Protoperidinium* cysts as indicators of
19 paleoproductivity in the northern Arabian Sea, *Mar. Micropaleontol.* 937, 1–13, 2003.

20 Schlanger, S.O., and Jenkyns, H.C.: Cretaceous oceanic anoxic events: Causes and
21 consequences, *Geologie en Mijnbouw*, 55, 179–184, 1976.

22 Schouten, S., Hopmans, E.C., Schefuss, E., and Sinninghe Damsté, J.S.: Distributional
23 variations in marine crenarchaeotal membrane lipids: a new tool for reconstructing ancient sea
24 water temperatures?, *Earth Planet. Sci. Lett.*, 204, 265-274, doi:10.1016/S0012-
25 821X(02)00979-2, 2002.

26 Schouten, S., Hopmans, E.C., Forster, A., van Breugel, Y., Kuypers, M.M.M., and Sinninghe
27 Damsté, J.S.: Extremely high sea-surface temperatures at low latitudes during the middle
28 Cretaceous as revealed by archaeal membrane lipids, *Geology*, 31, 1069–1072.
29 doi:10.1130/G19876.1, 2003.

30 Schouten, S., Hopmans, E.C., and Sinninghe Damsté, J.S.: The effect of maturity
31 and depositional redox conditions on archaeal tetraether lipid palaeothermometry, *Org.*
32 *Geochem.* 35, 567–571, doi:10.1016/j.orggeochem.2004.01.012, 2004.

33 Schouten, S., Huguet, C., Hopmans, E.C., Kienhuis, M.V.M., and Sinninghe Damsté: J.S.:
34 Improved analytical methodology for TEX₈₆ paleothermometry by high performance liquid

1 chromatography/atmospheric pressure chemical ionization-mass spectrometry, *Anal. Chem.*,
2 79, 2940–2944. doi:10.1021/ac062339v, 2007a.

3 Schouten, S., Forster, A., Panoto, F.E., and Sinninghe Damsté, J.S.: Towards calibration of
4 the TEX86 palaeothermometer for tropical sea surface temperatures in ancient greenhouse
5 worlds, *Org. Geochem.*, 38, 1537-1546, 2007b.

6 Schouten, S., Hopmans, E.C., and Sinninghe Damsté, J.S.: The organic geochemistry of
7 glycerol dialkyl glycerol tetraether lipids: a review. *Org. Geochem.*, 54, 19-61, 2013.

8 Sinninghe Damsté, J.S., Kenig, F., Koopmans, M.P., Köster, J., Schouten, S., Hayes, J.M.,
9 and de Leeuw, J.: Evidence for gammacerane as an indicator of water column stratification,
10 *Geochim. Cosmochim. Ac.*, 59, 1895–1900, doi:10.1016/0016-7037(95)00073-9, 1995.

11 Sinninghe Damsté, J.S., Kuypers, M.M.M., Pancost, R.D., and Schouten, S.: The carbon
12 isotopic response of algae, (cyano)bacteria, archaea and higher plants to the late Cenomanian
13 perturbation of the global carbon cycle: Insights from biomarkers in black shales from the
14 Cape Verde Basin (DSDP Site 367), *Org. Geochem.*, 39, 1703–1718,
15 doi:10.1016/j.orggeochem.2008.01.012, 2008.

16 Sinninghe Damsté, J.S., van Bentum, E.C., Reichart, G.-J., Pross, J., and Schouten, S.: A CO₂
17 decrease-driven cooling and increased latitudinal temperature gradient during the mid-
18 Cretaceous Oceanic Anoxic Event 2, *Earth Planet. Sc. Lett.*, 293, 97–103,
19 doi:10.1016/j.epsl.2010.02.027, 2010.

20 Sluijs, A., and Brinkhuis, H.: A dynamic climate and ecosystem state during the Paleocene-
21 Eocene Thermal Maximum: Inferences from dinoflagellate cyst assemblages on the New
22 Jersey shelf, *Biogeosciences*, 6, 1755–1781, doi:10.5194/bg-6-1755-2009, 2009.

23 Sluijs, A., Pross, J., and Brinkhuis, H.: From greenhouse to icehouse; organic-walled
24 dinoflagellate cysts as paleoenvironmental indicators in the Paleogene, *Earth-Sci. Rev.* 68,
25 281–315, doi:10.1016/j.earscirev.2004.06.001, 2005.

26 Snow, L.J., Duncan, R.A., and Bralower, T.J.: Trace element abundances in the Rock Canyon
27 anticline, Pueblo, Colorado, marine sedimentary section and their relationship to Caribbean
28 plateau construction and oxygen anoxic event 2, *Paleoceanography*, 20, PA3005,
29 doi:10.1029/2004PA001093, 2005.

30 Thomson, J.D.: Pollen transport and deposition by bumble bees in *Erythronium*: influences of
31 floral nectar and bee grooming, *J. Ecol.*, 74, 329-341. 1986.

32 Traverse, A., and Ginsburg, R.N.: Palynology of the surface sediments of Great Bahama
33 Bank, as related to water movement and sedimentation, *Mar. Geol.*, 4(6), 417-459, 1966.

1 Traverse, A.: Sedimentation of Organic Particles. Cambridge University Press, New York,
2 544 pp., 1994.

3 Tsikos, H., Jenkyns, H.C., Walsworth-Bell, B., Petrizzo, M.R., Forster, A., Kolonic, S., Erba,
4 E., Premoli Silva, I., Baas, M., Wagner, T., and Sinninghe Damsté, J.S.: Carbon-isotope
5 stratigraphy recorded by the Cenomanian–Turonian Oceanic Anoxic Event: correlation and
6 implications based on three key localities, *J. Geol. Soc. London*, 161, 711–719,
7 doi:10.1144/0016-764903-077,2004.

8 Turgeon, S.C., Creaser, R.A.: Cretaceous oceanic anoxic event 2 triggered by a massive
9 magmatic episode, *Nature*, 454, 323–326. doi:10.1038/nature07076, 2008.

10 Van Helmond, N.A.G.M., Sluijs, A., Reichert, G.J., Sinninghe Damsté, J.S., Slomp, C.P., and
11 Brinkhuis, H.: A perturbed hydrological cycle during Oceanic Anoxic Event 2, *Geology*, 42,
12 123–126, doi:10.1130/G34929.1, 2014.

13 Versteegh, G.J.M., and Zonneveld, K.A.F.: Use of selective degradation to separate
14 preservation from productivity, *Geology*, 30(7), 615–618, doi:10.1130/0091-7613(2002)
15 030<0615:UOSDTS>2.0.CO;2,2002.

16 Voigt, S., Gale, A.S., and Flögel, S.: Mid latitude shelf seas in the Cenomanian-Turonian
17 greenhouse world: Temperature evolution and North Atlantic circulation, *Paleoceanography*,
18 19, PA4020. doi:10.1029/2004PA001015, 2014.

19 Voigt, S., Gale, A.S., and Voigt, T.: Sea-level change, carbon cycling and palaeoclimate
20 during the Late Cenomanian of northwest Europe; An integrated palaeoenvironmental
21 analysis, *Cretaceous Res.*, 27, 836–858, doi:10.1016/j.cretres.2006.04.005, 2006.

22 Voigt, S., Erbacher, J., Mutterlose, J., Weiss, W., Westerhold, T., Wiese, F., Wilmsen, M.,
23 and Wonik, T.: The Cenomanian–Turonian of the Wunstorf section (north Germany): Global
24 stratigraphic reference section and new orbital time scale for oceanic anoxic event 2, *Newsl.*
25 *Stratigr.*, 43, 65–89, doi:10.1127/0078-0421/2008/0043-0065, 2008.

26 Wall, D., Dale, B., Lohmann, G.P., and Smith, W.K.: The environment and climatic
27 distribution of dinoflagellate cysts in modern marine sediments from regions in the North and
28 South Atlantic Oceans and adjacent seas, *Mar. Micropaleontol*, 2, 121–200, 1977.

29 Weijers, J.W.H., Schouten, S., Spaargaren, O.C., and Sinninghe Damsté, J.S.: Occurrence
30 and distribution of tetraether membrane lipids in soils: Implications for the use of the TEX₈₆
31 proxy and the BIT index, *Org. Geochem.*, 37, 1680–1693,
32 doi:10.1016/j.orggeochem.2006.07.018, 2006.

33 Wilmsen, M.: Sequence stratigraphy and palaeoceanography of the Cenomanian stage in
34 northern Germany, *Cretaceous Res.*, 24,525–568, doi:10.1016/S0195-6671(03)00069-7, 2003.

1 Zheng, X.-Y., Jenkyns, H.C., Gale, A.S., Ward, D.J., and Henderson, G.M.: Changing ocean
 2 circulation and hydrothermal inputs during Oceanic Anoxic Event 2 (Cenomanian–Turonian):
 3 Evidence from Nd-isotopes in the European shelf sea, *Earth Planet. Sc. Lett.*, 375, 338-348.
 4 doi.org/10.1016/j.epsl.2013.05.053i, 2013.

5 Zonneveld, K.A.F., Versteegh, G.J.M., and De Lange, G.J.: Preservation of organic walled
 6 dinoflagellate cysts in different oxygen regimes: a 10,000 yr natural experiment, *Mar.*
 7 *Micropaleontol.*, 29, 393–405, doi:10.1016/S0377-8398(96)00032-1,1997.

8 Zonneveld, K.A.F., Versteegh, G.J.M., and De Lange, G.J.: Palaeoproductivity and post-
 9 depositional aerobic organic matter decay reflected by dinoflagellate cyst assemblages of the
 10 Eastern Mediterranean S1 sapropel, *Mar. Geology*, 172, 181–195, 2001.

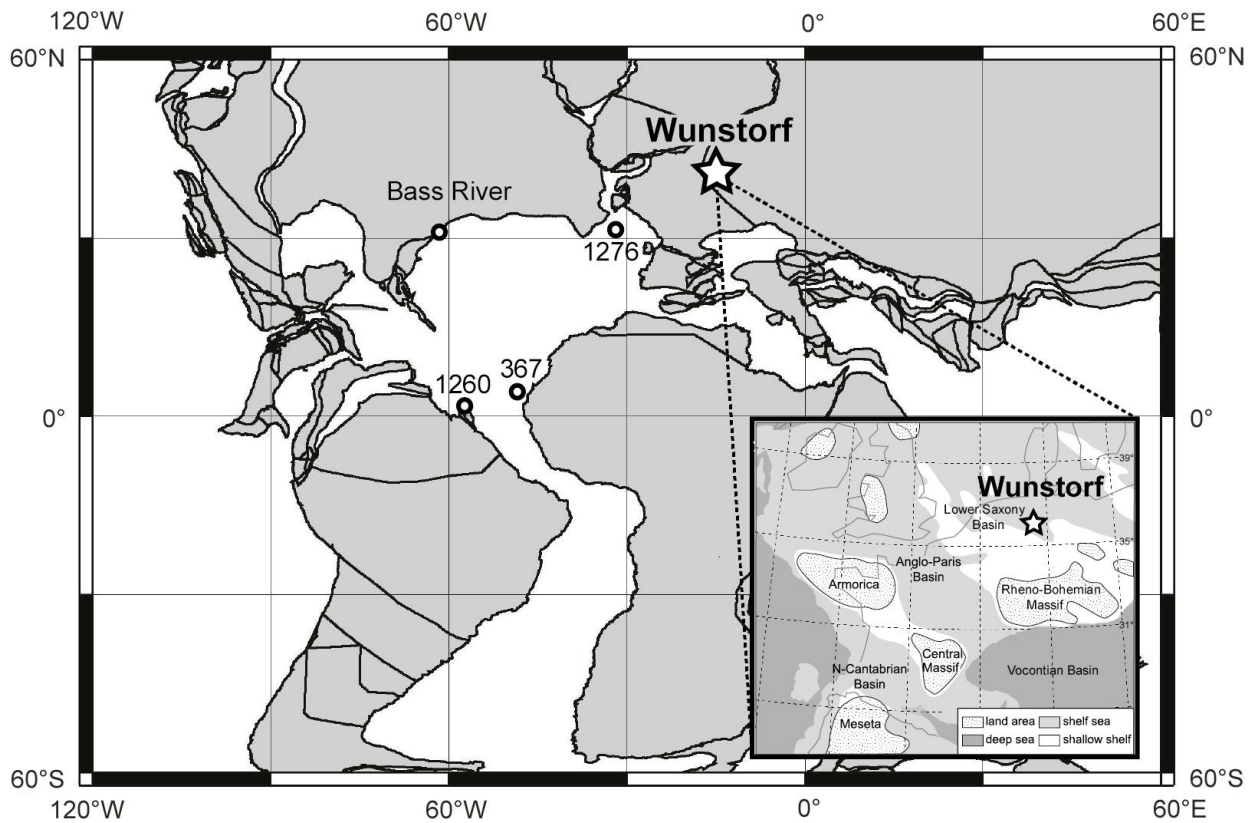
11
 12
 13
 14
 15
 16
 17

18 Table 1. Overview of the different sites for which TEX₈₆-paleothermometry was applied over the
 19 OAE2-interval, and TEX₈₆ values and paleo-SST ranges and averages.

Site	Estimated paleolatitude	TEX ₈₆ range (average)	Reconstructed paleo-SST ^a range (average)
ODP Site 367 ^b	5°N	0.84-0.95 (0.90)	33-37°C (36°C)
ODP Site 1260 ^b	0°	0.85-0.95 (0.92)	34-37°C (36°C)
ODP Site 1276 ^c	30°N	0.74-0.96 (0.90)	30-37°C (36°C)
Bass River ^d	30°N	0.84-0.95 (0.91)	33-37°C (36°C)
Wunstorf	40°N	0.80-0.99 (0.93)	32-38°C (36°C)

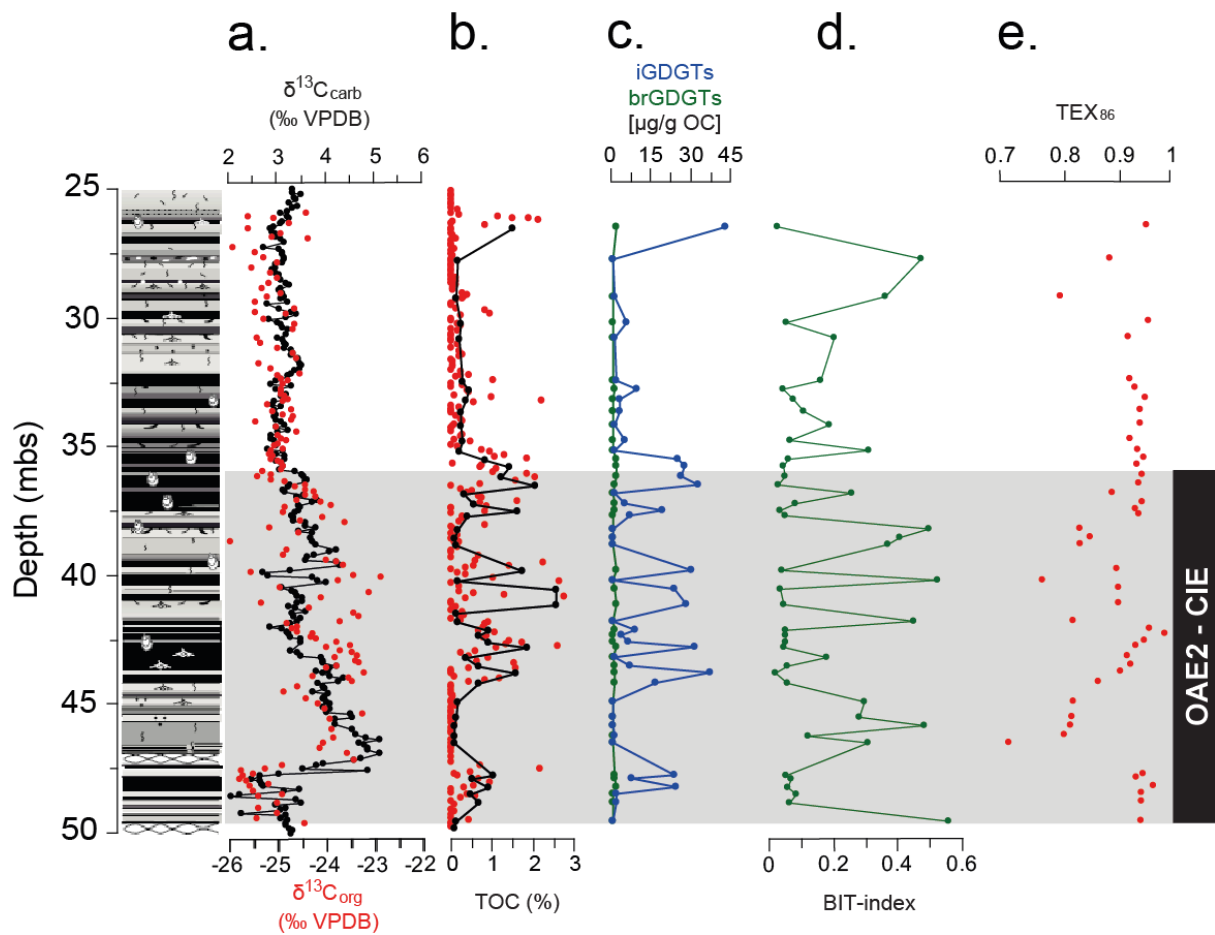
20
 21
 22
 23
 24
 25

^a Based on the TEX₈₆^H calibration by Kim et al., 2010, ^b Forster et al., 2007, ^c Sinninghe Damsté et al.,
 2010, ^d van Helmond et al., 2014



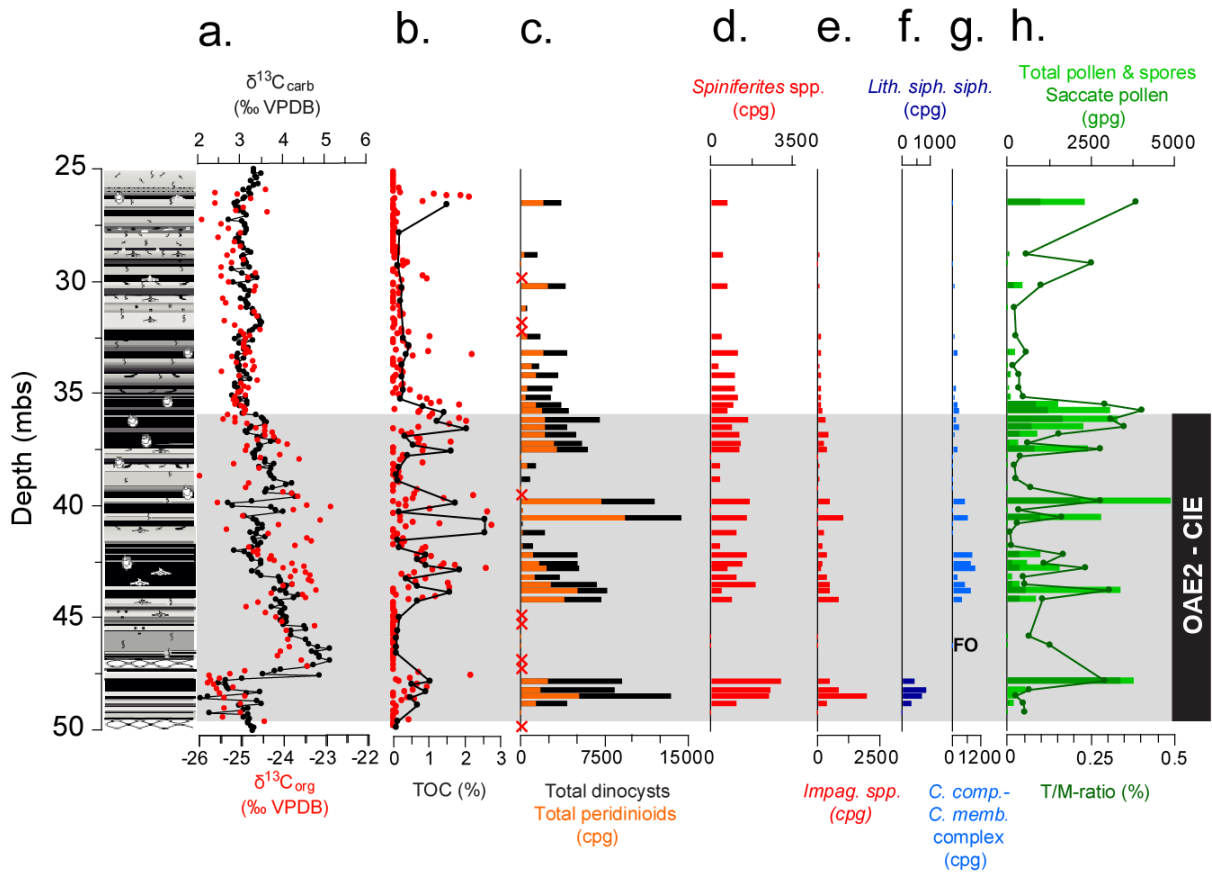
1
2
3
4
5
6
7
8
9

Figure 1. Paleotectonic reconstruction for the Cenomanian/Turonian boundary time interval, with the location of the Wunstorf core and sections with previously published TEX_{86} -based SST-records: Bass River, DSDP site 367, ODP sites 1260 and 1276 indicated (map generated at <http://www.odsn.de/odsn/services/paleomap/paleomap.html>). Inset map shows a detailed paleogeographic reconstruction of central and western Europe, including the location of the Wunstorf core (modified from Voigt et al., 2004).

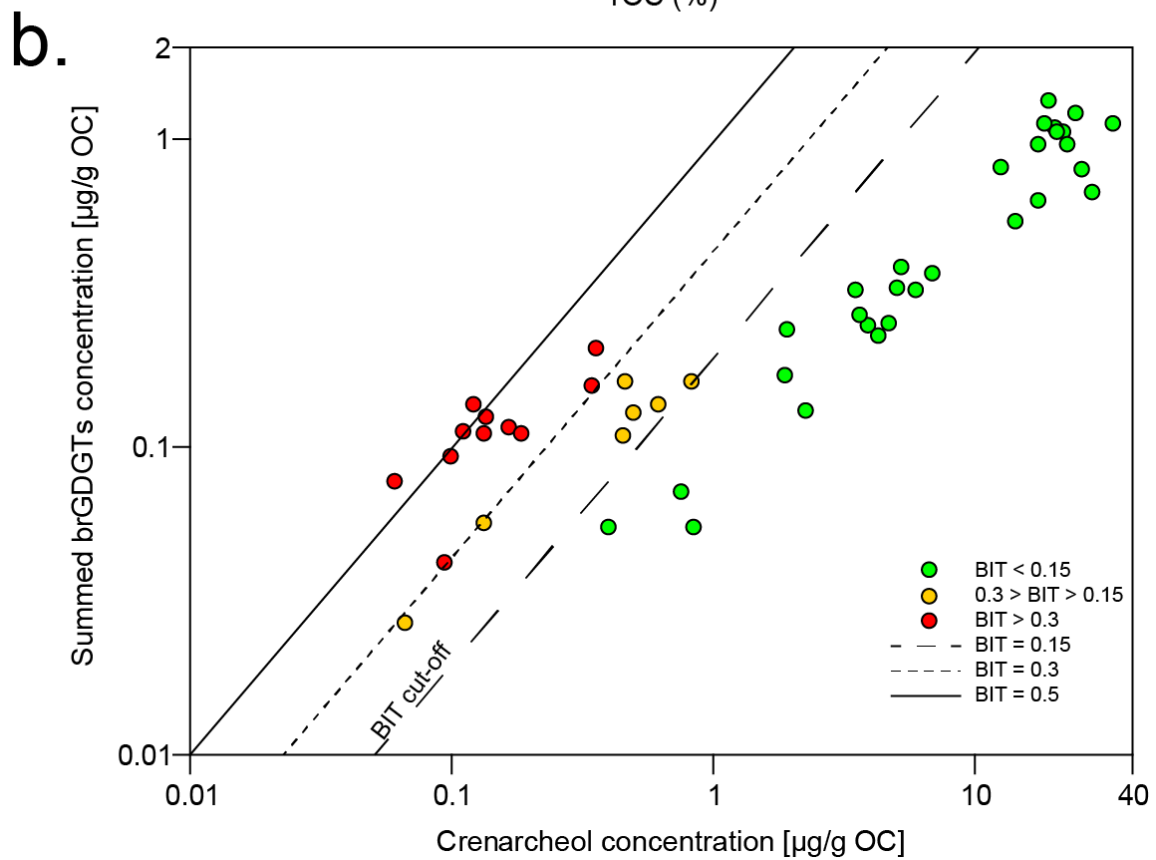
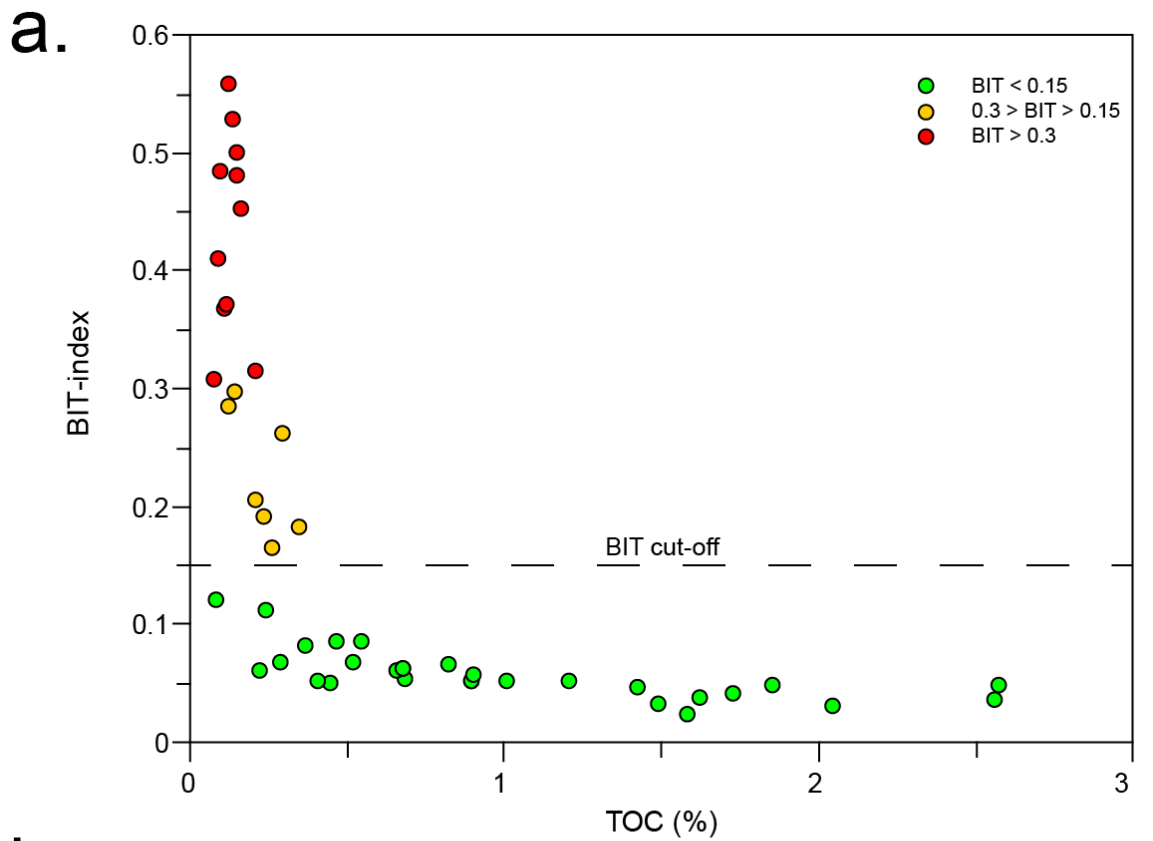


1
 2 Figure 2. Geochemical results for the Cenomanian-Turonian transition of the Wunstorf core.
 3 Stratigraphy from Voigt et al.(2008). (a) $\delta^{13}\text{C}_{\text{carb}}$ (Voigt et al., 2008) and $\delta^{13}\text{C}_{\text{org}}$ (du Vivier et
 4 al., 2014; red). (b) Total organic carbon (TOC; black, this study; red, Hetzel et al., 2011). (c)
 5 concentrations of summed iGDGTs and summed brGDGTs [$\mu\text{g/g OC}$].(d) BIT-index. (e)
 6 TEX_{86} -values. The grey zone indicates the OAE2 interval after Voigt et al.(2008). mbs =
 7 meters below surface.

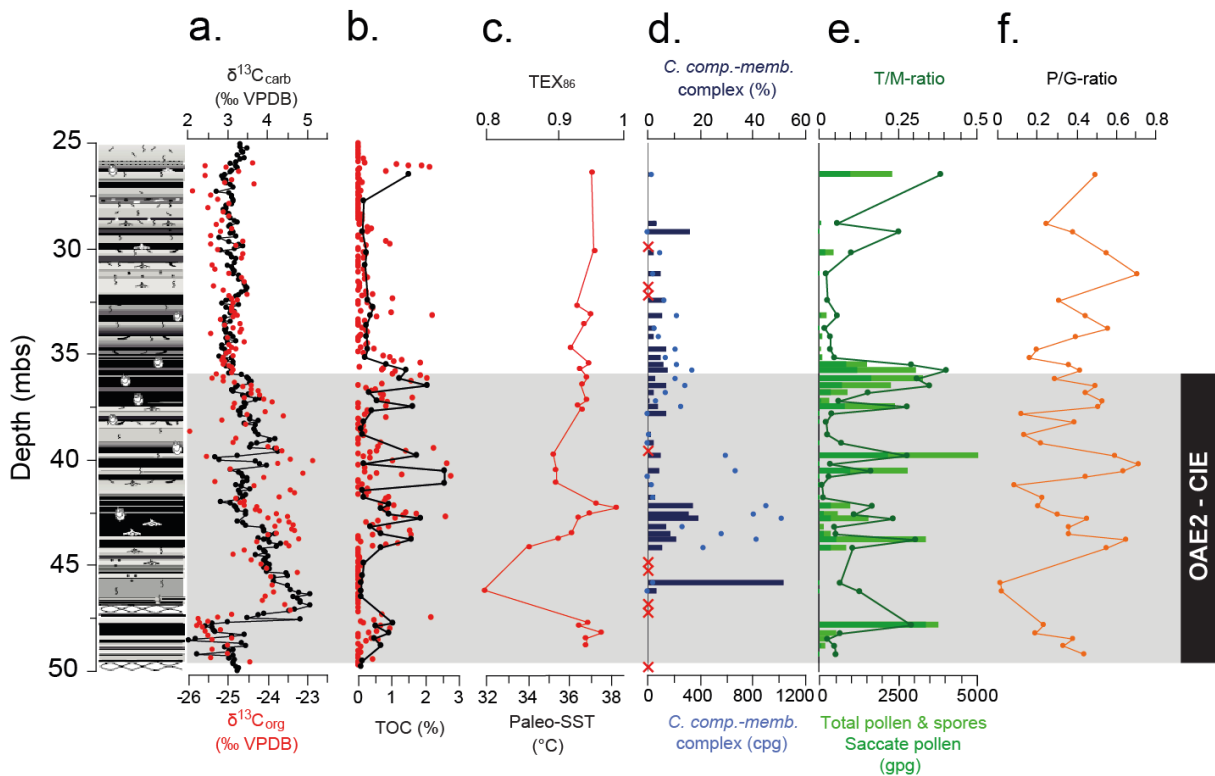
8
 9



1 Figure 3. Geochemical and palynological results for the Cenomanian-Turonian transition of
 2 the Wunstorf core. Stratigraphy from Voigt et al. (2008). (a) $\delta^{13}\text{C}_{\text{carb}}$ (Voigt et al., 2008) and
 3 $\delta^{13}\text{C}_{\text{org}}$ (du Vivier et al., 2014; red). (b) Total organic carbon (TOC; black, this study; red,
 4 Hetzel et al., 2011). (c) Total dinocyst concentrations (black) and total peridinioidal cysts
 5 (orange) per gram sediment dry weight (cp/g). (d) Dinocyst species *Spiniferites* spp. (cp/g). (e)
 6 Dinocyst species *Impagidinium* spp. (cp/g). (f) Dinocyst species *Lithosphaeridium*
 7 *siphoniphorum siphoniphorum* (cp/g). (g) Dinocyst species *Cyclonephelium compactum* – *C.*
 8 *membraniphorum* complex (cp/g). (h). Terrestrial vs. marine palynomorphs (T/M-ratio) and
 9 total pollen and spores in grains per dry gram of sediment (gpg), saccate gymnosperm pollen
 10 in dark green. The grey zone indicates the OAE2 interval after Voigt et al. (2008). mbs =
 11 meters below surface.



1
 2 Figure 5. (a) Cross plot of summed brGDGTs ($\mu\text{g/g OC}$) versus crenarcheol ($\mu\text{g/g OC}$) on a
 3 logarithmic axis. (b) Cross plot of BIT-index values versus total organic carbon (TOC).



1
 2 Figure 6. Geochemical and palynological results for the Cenomanian-Turonian transition of
 3 the Wunstorf core. Stratigraphy from Voigt et al. (2008). (a) $\delta^{13}\text{C}_{\text{carb}}$ (Voigt et al., 2008) and
 4 $\delta^{13}\text{C}_{\text{org}}$ (du Vivier et al., 2014; red). (b) Total organic carbon (TOC; black, this study; red,
 5 Hetzel et al., 2011). (c) TEX_{86} -values and $\text{TEX}_{86}^{\text{H}}$ -based SST reconstruction (Kim et al.,
 6 2010) (d) Relative abundance (%) and absolute abundance in cysts per dry gram of sediment
 7 (cpg), of the dinocyst species *Cyclonephelium compactum*- *C. membraniphorum* complex,
 8 'X' represents barren samples. (e) Terrestrial vs. marine palynomorphs (T/M-ratio) and total
 9 pollen and spores in grains per dry gram of sediment (gpg), saccate gymnosperm pollen in
 10 dark green (f) Peridinioid vs. gonyaulacoid dinocysts (P/G-ratio). The grey zone indicates the
 11 OAE2 interval after Voigt et al. (2008). mbs = meters below surface.